Spatial evolution of magnetic reconnection diffusion region structures with distance from the X-line

Cite as: Phys. Plasmas 28, 122901 (2021); https://doi.org/10.1063/5.0072182 Submitted: 20 September 2021 • Accepted: 09 November 2021 • Published Online: 02 December 2021











Physics of Plasmas Papers from 62nd Annual Meeting of the APS Division of Plasma Physics



Read now!

Spatial evolution of magnetic reconnection diffusion region structures with distance from the X-line

Cite as: Phys. Plasmas **28**, 122901 (2021); doi: 10.1063/5.0072182 Submitted: 20 September 2021 · Accepted: 9 November 2021 · Published Online: 2 December 2021







M. Øieroset, ^{1,a)} D. D. Phan, D. R. Ergun, D. N. Ahmadi, D. K. Genestreti, D. J. F. Drake, D. Y.-H. Liu, C. Haggerty, D. P. Eastwood, D. M. A. Shay, D. P. S. Pyakurel, S. Haaland, D. M. Oka, D. M. Goodbred, S. Eriksson, D. J. L. Burch, D. R. B. Torbert, P. Y. Khotyaintsev, C. T. Russell, R. J. Strangeway, D. J. Gershman, D. J. Ger

AFFILIATIONS

Note: This paper is a part of the Special Collection: Plasma Physics from the Magnetospheric Multiscale Mission.

ABSTRACT

We report Magnetospheric Multiscale four-spacecraft observations of a thin reconnecting current sheet with weakly asymmetric inflow conditions and a guide field of approximately twice the reconnecting magnetic field. The event was observed at the interface of interlinked magnetic field lines at the flank magnetopause when the maximum spacecraft separation was 370 km and the spacecraft covered \sim 1.7 ion inertial lengths (d_i) in the reconnection outflow direction. The ion-scale spacecraft separation made it possible to observe the transition from electron-only super ion-Alfvénic outflow near the electron diffusion region (EDR) to the emergence of sub-Alfvénic ion outflow in the ion diffusion region (IDR). The EDR to IDR evolution over a distance less than 2 d_i also shows the transition from a near-linear reconnecting magnetic field reversal to a more bifurcated current sheet as well as significant decreases in the parallel electric field and dissipation. Both the ion and electron heating in this diffusion region event were similar to the previously reported heating in the far downstream exhausts. The dimensionless reconnection rate, obtained four different ways, was in the range of 0.13–0.27. This event reveals the rapid spatial evolution of the plasma and electromagnetic fields through the EDR to IDR transition region.

© 2021 Author(s). All article content, except where otherwise noted, is licensed under a Creative Commons Attribution (CC BY) license (http://creativecommons.org/licenses/by/4.0/). https://doi.org/10.1063/5.0072182

¹Space Sciences Laboratory, University of California, Berkeley, California 94720, USA

²University of Colorado LASP, Boulder, Colorado 80303, USA

³Space Science and Engineering, Southwest Research Institute, Durham, New Hampshire 03824, USA

⁴University of Maryland, College Park, Maryland 20742, USA

⁵Dartmouth College, Hanover, New Hampshire 03755, USA

⁶University of Hawaii, Honolulu, Hawaii 96822, USA

⁷The Blackett Laboratory, Imperial College London, London SW7 2BX, United Kingdom

⁸Department of Physics and Astronomy, University of Delaware, Newark, Delaware 19716, USA

⁹Birkeland Centre for Space Science, University of Bergen, 5007 Bergen, Norway

¹⁰Max-Planck Institute for Solar Systems Research, 37077 Göttingen, Germany

[&]quot;Southwest Research Institute, San Antonio, Texas 78238, USA

¹²University of New Hampshire, Durham, New Hampshire 03824, USA

¹³Swedish Institute of Space Physics, 75237 Uppsala, Sweden

¹⁴University of California, Los Angeles, Los Angeles, California 90095, USA

¹⁵NASA Goddard Space Flight Center, Greenbelt, Maryland 20771, USA

a) Author to whom correspondence should be addressed: oieroset@berkeley.edu

I. INTRODUCTION

Magnetic reconnection is a universal plasma process that converts magnetic energy to particle energy. For standard reconnection to occur, both electrons and ions decouple from the magnetic field, and the dissipation region develops a two-scale structure: An inner electron diffusion region (EDR) with electron skin depth scales where the electron flow completely dominates those of the ions and the electron frozen-in condition is broken, and an outer ion diffusion region (IDR) with ion inertial length (d_i) scales (e.g., Vasyliunas, 1975; Sonnerup, 1979; Shay et al., 1998). In the IDR, electrons are frozen-in to the magnetic field, but the ions are not, leading to Hall magnetic and electric fields (e.g., Sonnerup, 1979).

The predicted Hall magnetic and electric fields in the IDR have been confirmed by numerous spacecraft observations (e.g., Nagai et al., 2001; Øieroset et al., 2001; Mozer et al., 2002; Runov et al., 2003; Borg et al., 2005; Eastwood et al., 2010a). However, observing the miniscule EDR remained a challenge until the launch of NASA's Magnetospheric Multiscale (MMS) mission, a four-spacecraft mission designed to study magnetic reconnection at the electron scale, with unprecedented high time resolution measurements and electron-scale spacecraft separation (Burch et al., 2016a). MMS has indeed provided conclusive evidence for electron demagnetization in the electron diffusion region (EDR) where reconnection of magnetic fields takes place (e.g., Burch et al., 2016b; Chen et al., 2016; Burch and Phan, 2016; Torbert et al., 2016, 2018; Eriksson et al., 2016; Genestreti et al., 2017; Webster et al., 2018).

The transition from the EDR to the IDR has been studied in kinetic simulations, which predict super-Alfvénic electron outflow jets close to the X-line followed by a decrease in the electron outflow speed through the IDR away from the X-line (e.g., Hesse *et al.*, 1999; Shay *et al.*, 1999). Further downstream, the ions are gradually accelerated away through the IDR and when electrons and ions reach a joint outflow speed (approximately the Alfvén speed), it marks the exit from the IDR into the ion and electron coupled exhaust.

The super-Alfvénic electron jets near the X-line and their slowing down further away have been observed in the magnetotail when spacecraft cross an X-line along the outflow direction (Nagai *et al.*, 2011; Zenitani *et al.*, 2011; Torbert *et al.*, 2018). However, with such a trajectory, one cannot study how the cross-current sheet plasma and field profiles evolve with distances from the X-line.

In this paper, we present a fortuitous Magnetospheric Multiscale (MMS) observation with ion-scale spacecraft separation across a thin reconnecting current sheet. The unusually large (up to 370 km) separation occurred during orbit adjustments from the nightside to the dayside phase of the MMS mission in October 2017. The ion-scale spacecraft separation made it possible to study the spatial evolution of the cross-current-sheet profiles of the reconnection layer in the EDR–IDR-exhaust transition region.

The event was observed during an MMS traversal of a compressed, thin current sheet at the interface of interlinked magnetic field lines emanating from two X-lines at the flank magnetopause. Recent observations have shown that reconnection can occur in such current sheets (Øieroset et al., 2016, 2019; Kacem et al., 2018; Fargette et al., 2020a; Russell and Qi, 2020). Although the reconnection event is at the magnetopause, which one would usually associate with asymmetric reconnection, this type of interlinked reconnection is closer to being symmetric, as the properties of the two inflowing plasmas tend to be rather similar.

The paper is organized as follows. Section II describes the MMS instrumentation. Section III describes the large-scale context of the event. The current sheet (LMN) coordinate system is presented in Sec. IV, while Sec. V discusses the reconnection geometry. Section VI shows the inflow conditions, and Sec. VII contrasts the current sheet profiles at the four spacecraft. The key findings are summarized and discussed in Sec. VIII.

II. INSTRUMENTATION

We use MMS Level 2 (L2) flux gate magnetometer (FGM) data at 128 samples/s (Russell *et al.*, 2014) and fast plasma investigation (FPI) data at 30 ms resolution for electrons and 150 ms for ions (Pollock *et al.*, 2016). For the electric field (Torbert *et al.*, 2014), we use Level 3 (L3) data at 8192 samples/s. The L3 data are calibrated using burst FPI data comparing the electric field with $-V \times B$ to remove the offsets and adjust the baseline while L2 electric field data use the fast FPI data for calibration.

III. LARGE-SCALE CONTEXT

Figure 1 shows MMS1 observations, in GSE coordinates, of a magnetic flux enhancement event at the dusk flank magnetopause, at GSE ($-6.8 \text{ R}_{\text{E}}$, $19.8 \text{ R}_{\text{E}}$, 6.2 R_{E}). The upstream interplanetary magnetic field associated with this event was $B_{GSE} = (5, -4, 1)$ nT. A sharp polarity reversal in B_Y [Fig. 1(b), green curve] was observed by MMS at 03:55:18 UT, near the time of maximum $|\mathbf{B}|$, indicating the presence of a thin current sheet. The magnitude of By was enhanced on both sides of the thin current sheet. The transition across the thin current sheet shows an abrupt change of the pitch-angle distributions of 0.1–1 keV electrons [Fig. 1(e)], with counterstreaming electrons to the left and predominantly antifield-aligned electrons to the right, indicating that the plasmas on the two sides of the current sheet were not magnetically connected. The observed magnetic field enhancement with an embedded thin current sheet separating two regions of different magnetic topology is qualitatively similar to previous observations interpreted as interlinked magnetic fields (e.g., Kacem et al., 2018; Øieroset et al., 2016, 2019; Fargette et al., 2020a, 2020b) or interlinked flux ropes (Russell and Qi, 2020). Figure 1, panels (l) and (m), illustrates the envisioned scenario of how two magnetic field lines, originating from different X-lines, collide and form a thin current sheet when they become interlinked.

Inside the thin interface current sheet at \sim 03:55:18 UT, MMS1 observed enhanced current density up to \sim 0.4 μ A m⁻² [Fig. 1(k)]. In the following Secs. (IV–VII), we present the detailed multispacecraft observations and show that the thin current sheet underwent reconnection.

IV. LMN COORDINATE SYSTEM AND SPACECRAFT SEPARATION

The thin current sheet observations are presented in the current sheet (LMN) coordinate system determined by minimum variance analysis of the magnetic field (Sonnerup and Cahill, 1967) across the current sheet: the current sheet normal points along N, L is along the antiparallel magnetic field direction, and $\mathbf{M} = \mathbf{N} \times \mathbf{L}$ is in the out-of-plane ("X-line") direction. To facilitate the comparisons between the observations from the four spacecraft, we use a common LMN, L = GSE (-0.0003, 0.997, 0.0632), M = GSE (0.774, -0.0395, 0.631), N = GSE (0.632, 0.0486, -0.772), obtained by averaging the four individual LMN coordinates determined at each spacecraft current sheet crossing. The maximum difference between the average and individual

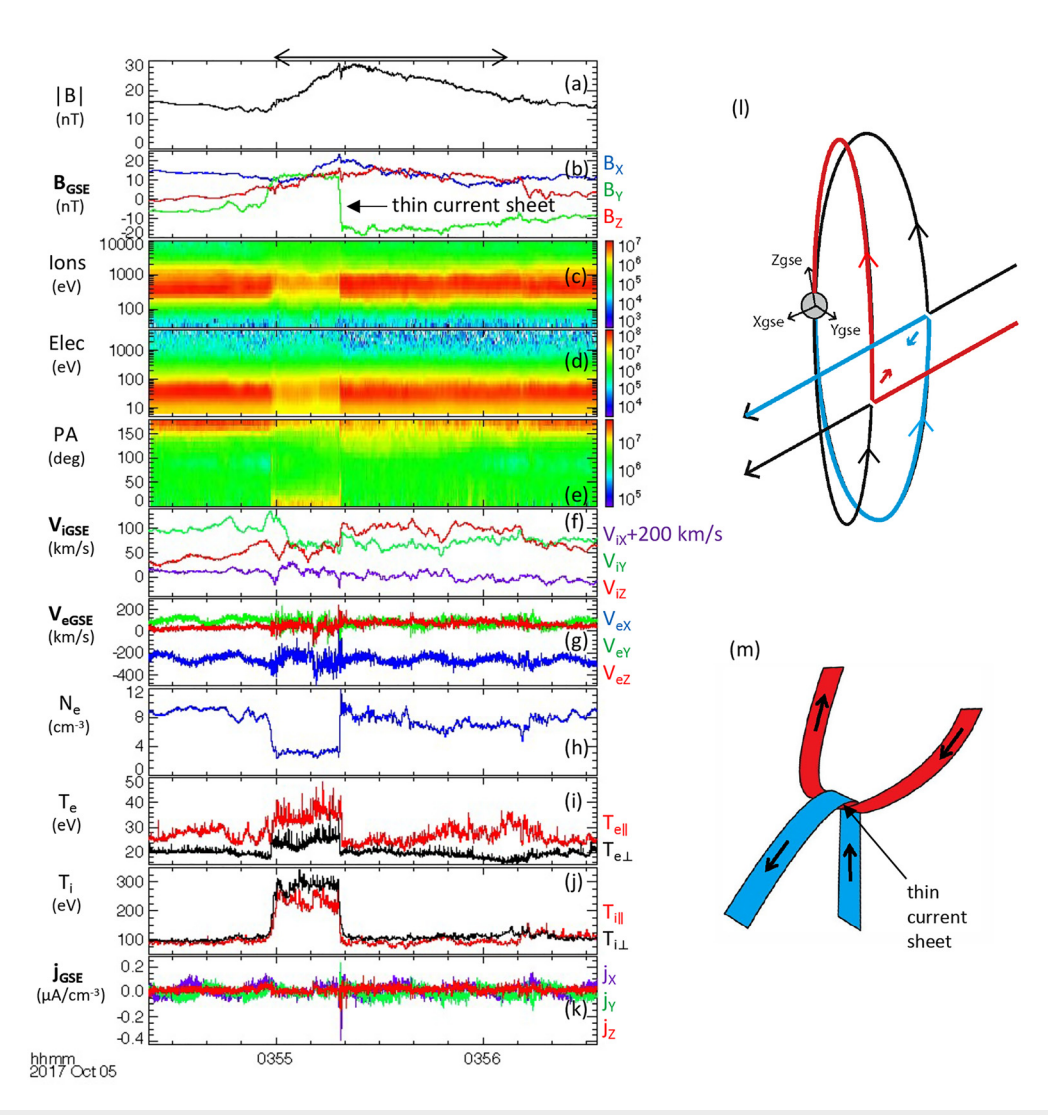


FIG. 1. (a)—(k) MMS1 observations of the large-scale context of the event, in GSE. Interval of enhanced magnetic field is marked with the horizontal double arrow. (a) and (b) Magnetic field magnitude and components, (c) ion energy flux, (d) electron energy flux, (e) pitch angle spectrogram for 0.1–1 keV electrons, (f) ion velocity, (g) electron velocity, (h) electron density, (i) electron temperature, (j) ion temperature, (k) current density calculated using plasma data, $j = eN_e (V_i - V_e)$, (l) sketch illustrating how reconnection at two locations at the magnetopause can lead to converging plasma jets and interlinked magnetic field lines, and (m) interlinked magnetic field lines forming a thin current sheet.

LMN vectors was only 2° , supporting the use of a common LMN coordinate system.

The event was encountered at the dusk tail flank on 2017-10-05 at around 03:55:18 UT, at GSE ($-6.8~R_{\rm E}$, $19.8~R_{\rm E}$, $6.2~R_{\rm E}$). The maximum spacecraft separation was 370 km (4 $d_{\rm i}$), with a maximum separation along L of 42 km, along M of 219 km, and along N of 296 km. However, due to the tangential $V_{\rm L}$ flow and the assumed associated X-line drift speed of $88~{\rm km/s}$, the effective spacecraft separation along L during the current sheet crossing was $163~{\rm km}$, or $1.7~d_{\rm i}$ (see Sec. VI).

V. RECONNECTION LAYER GEOMETRY

We now present the detailed four-spacecraft observations of the thin current sheet in LMN coordinates and deduce the reconnection geometry. All spacecraft observed a transition in B_L from $\sim\!+12$ to $\sim\!-13$ nT across the current sheet [Fig. 2(a)]. The dashed vertical lines denote the well-defined times when B_L started to change from its asymptotic values, i.e., the current sheet edges. The dotted vertical line shows the current sheet midplane, i.e., where $B_L=0$. The B_L reversal was first encountered by MMS4 (blue), followed by MMS3 (green), MMS2 (red), and MMS1 (black). The current sheet moved tailward with the magnetosheath flow in the negative X_{GSE} direction [Figs. 1(f) and 1(g)] and the negative N direction, i.e., the motion of MMS relative to the current sheet must be in the +N direction [Figs. 2(k) and 2(l)]. Several plasma and magnetic field features indicate that all four spacecraft crossings of the current sheet occurred to the left of an X-line in the reconnection geometry sketched in Figs. 2(k) and 2(l):

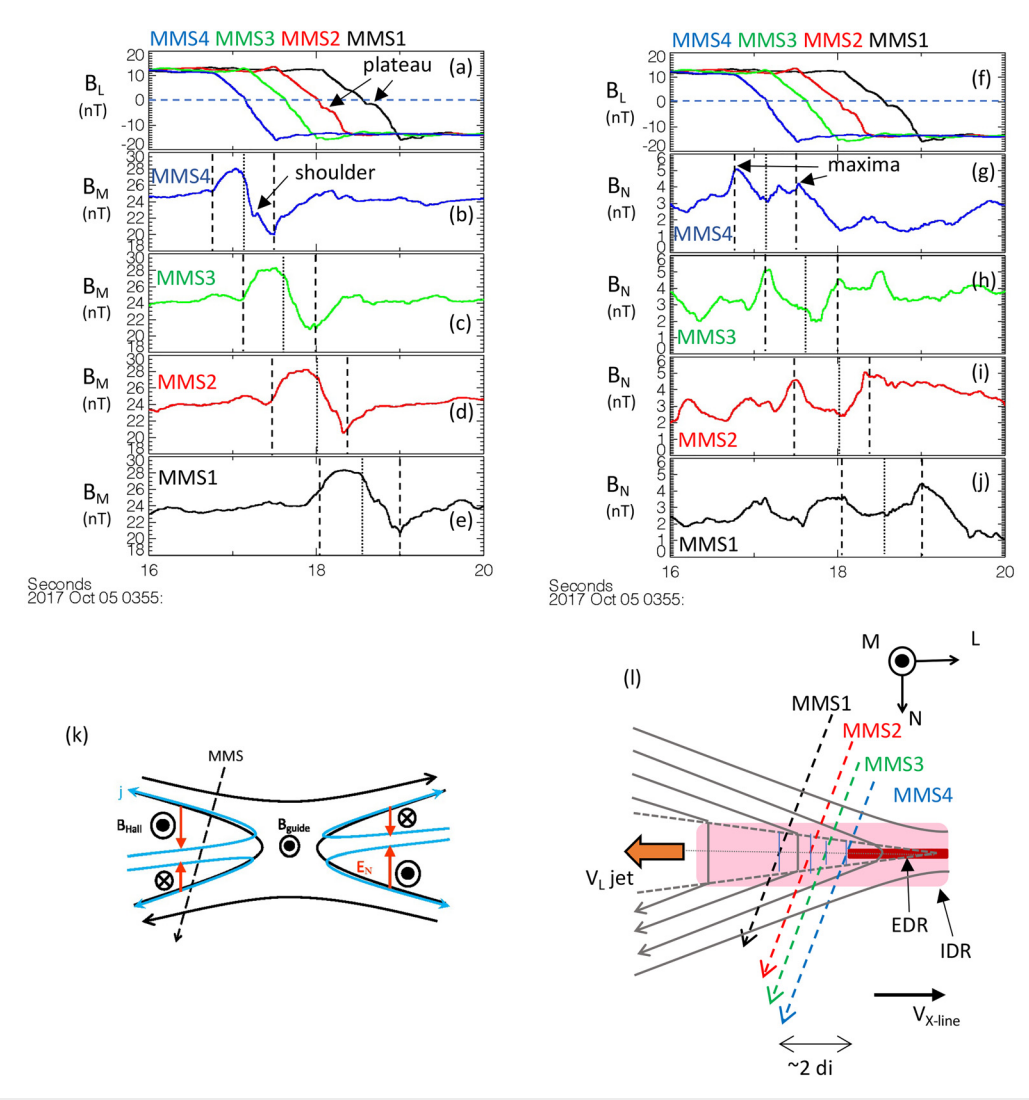


FIG. 2. Detailed multispacecraft observations of the thin current sheet in LMN coordinates. (a) and (f) Reconnecting magnetic field BL for all four spacecraft, (b)–(e) and (g)–(j) BM and BN for each spacecraft, (k) cartoon showing the quadrupolar Hall currents (blue) and Hall magnetic fields, (l) sketch of the reconnection layer with magnetic field lines (black), EDR (red), IDR (pink), and approximate MMS spacecraft trajectories. Vertical dashed lines in the time series (a)–(j) and (g)–(j) mark the current sheet edges and the vertical dotted lines the current sheet midplane (BL = 0).

- 1. A positive to negative bipolar variation in B_M relative to the guide field of \sim 24 nT was observed at all four spacecraft [Figs. 2(b)–2(e)], consistent with the expected quadrupolar out-of-plane Hall magnetic fields to the left of the X-line (e.g., Sonnerup, 1979; Øieroset et al., 2001; Mozer et al., 2002) [Fig. 2(k)]. With the relatively strong guide field, the signature should be asymmetric with a larger $+B_M$ perturbation (Pritchett, 2001; Eastwood et al., 2010b), which is what is seen.
- Consistent with all four spacecraft crossing the reconnecting current sheet to the left of the X-line, B_N was positive at all the spacecraft [Figs. 2(g)-2(j)], although its magnitude was not constant.
- 3. An enhancement in V_{eL} (compared to external flows) was observed at all four spacecraft in the negative L direction at the current sheet midplane ($B_L=0$, dotted vertical lines), consistent

- with all four spacecraft crossing the current sheet to left of the X-line [Figs. 3(g)-3(j)].
- 4. Two of the spacecraft (MMS 2 and 1) detected outflow V_{iL} jets. The ion jet direction was in the negative L direction at the current sheet midplane ($B_L=0$, dotted vertical lines), also consistent with the two spacecraft being located to the left of the X-line [Figs. 3(d) and 3(e)].
- 5. The observed current sheet duration increased from MMS4 to MMS1. The observed current sheet duration at MMS4, MMS3, MMS2, and MMS1, respectively, was 0.760, 0.905, 0.94, and 1.01 s. Considering the locations of the four spacecraft relative to each other along L, the systematic differences in the current sheet crossing durations are consistent with the widening of the left-side exhaust with distance from the X-line.

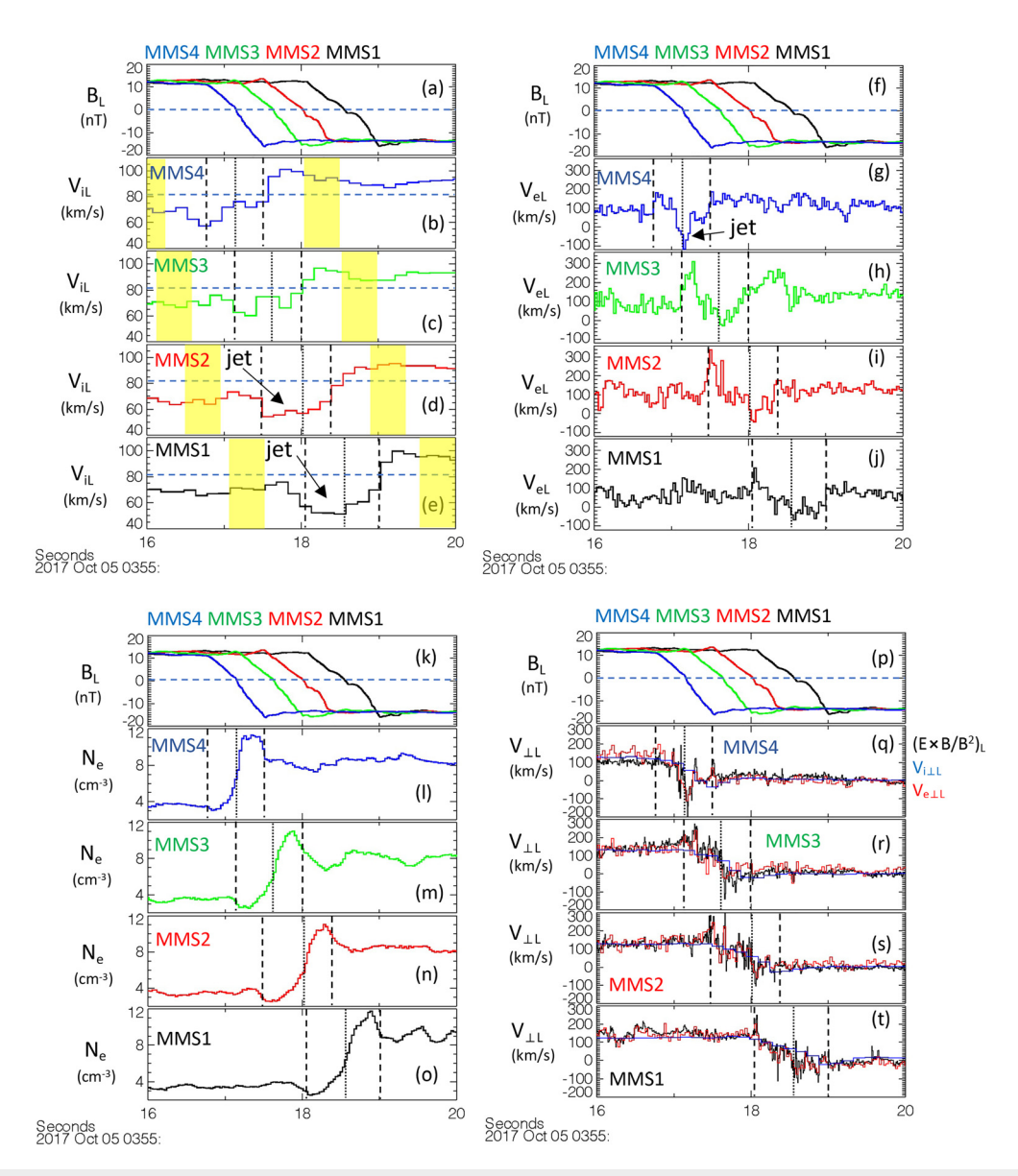


FIG. 3. Detailed multispacecraft observations of the thin current sheet in LMN coordinates. (a), (f), (k), and (p) Reconnecting magnetic field B_L for all four spacecraft, (b)–(e) and (g)–(j) $V_{i,L}$ and $V_{e,L}$ for each spacecraft, (l)–(o) electron density for each spacecraft, (q)–(t) $V_{i,L,L}$ (blue), $V_{e,L,L}$ (red), and ($E \times B/B^2$)_L (black) for each spacecraft. Vertical dashed lines in the time series mark the current sheet edges and the vertical dotted lines the current sheet midplane ($B_L = 0$). Intervals used to calculate the average inflow parameters are marked in yellow in (b)–(e).

The observed parameters from all four spacecraft are summarized in Table I. In the following Secs. (VI and VII), we first discuss the inflow parameters and then the evolution of the outflow structure.

VI. INFLOW CONDITIONS

The inflow parameters are to be sampled outside of the current sheet. Ideally, one would choose a stable interval right outside the current sheet edges. However, close to the X-line, the ion outflows can extend outside the current sheet (e.g., Øieroset et al., 2019). Thus, in order to sample the true inflow (asymptotic) conditions, one needs to

pick the inflow regions slightly away from the current sheet edges on both sides. Based on the examination of the ion velocity at the four spacecraft, and for simplicity, we chose the inflow intervals [shaded in yellow in Figs. 3(b)-3(e)] to be of 0.5 s duration, taken 0.5 s away from the current sheet edges. We also verified that most of the plasma and field parameters were relatively stable in the chosen intervals. The inflow parameter values are given in Table I. For most of the conclusions of the paper, the inflow parameters do not need to be highly accurate.

The inflow plasma and field conditions were weakly asymmetric, with a factor of \sim 2 difference in the inflow density [Figs. 3(1)–3(o)],

TABLE I. Observed inflow and outflow parameters for the 2017-10-05/03:55:18 UT reconnecting current sheet event.

	MMS1	MMS2	MMS3	MMS4
$\overline{N_{\text{in},1}}$	$3.5\mathrm{cm}^{-3}$	$3.5\mathrm{cm}^{-3}$	$3.4{\rm cm}^{-3}$	$3.5\mathrm{cm}^{-3}$
$N_{in,2}$	9.0cm^{-3}	$8.6\mathrm{cm}^{-3}$	$8.6\mathrm{cm}^{-3}$	7.9cm^{-3}
$B_{in,L1}$	12.5 nT	12.7nT	12.6 nT	12.3nT
$B_{in,L2}$	13.6nT	13.6nT	13.1nT	13.4nT
$V_{i,in,L1}$	71 km/s	65 km/s	69 km/s	67 km/s
$V_{i,in,L2}$	95 km/s	94 km/s	89 km/s	95 km/s
$T_{i,in,1}$	264 eV	246 eV	247 eV	245 eV
$T_{i,in,2}$	108 eV	110 eV	114 eV	116 eV
$T_{e,in,1}$	29 eV	30 eV	30 eV	30 eV
$T_{e,in,2}$	21 eV	21 eV	21 eV	21 eV
$V_{AL,hybrid}$	115 km/s	117 km/s	114 km/s	118 km/s
d_i	92 km	93 km	93 km	96 km
$N_{in,hybrid}$	6.1cm^{-3}	$5.9\mathrm{cm}^{-3}$	$6.0\mathrm{cm}^{-3}$	5.6cm^{-3}
$T_{i,in,hybrid}$	154 eV	151 eV	153 eV	158 eV
$T_{e,in,hybrid}$	24eV	24 eV	24 eV	24 eV
V _{iL,X-line_drift}	88 km/s	85 km/s	83 km/s	86 km/s
$T_{i_ave_exhaust}$	172 eV	171 eV	170 eV	170 eV
$T_{e_ave_exhaust}$	26 eV	27 eV	26 eV	26 eV
$E_{M_ave_exhaust}$	$-0.08\pm0.37~\mathrm{mV/m}$	$-0.25\pm0.40~\mathrm{mV/m}$	$-0.07 \pm 0.64 \mathrm{mV/m}$	$-0.14 \pm 0.54 \text{ mV/m}$
$B_{N_ave_exhaust_inflow}$	$2.7 \pm 0.8 \text{ nT}$	3.6 nT \pm 0.8 nT	$3.4\pm0.8~\mathrm{nT}$	$3.1 \pm 0.9 \text{ nT}$
Reconnection rate from $B_{N_ave_exhaust_inflow}$	0.20	0.27	0.26	0.24

annilow parameters from the two inflow regions (subscripts "1" and "2") were averaged over a 0.5 s interval obtained 0.5 s before and after the current sheet edges (yellow shaded area in Figs. 3(b)-3(e). Subscript "ave_exhaust" indicates the average value across the current sheet from edge to edge, except for E_M and B_N where the average was taken from inflow to inflow. $V_{AL,hybrid}$, $N_{in,hybrid}$, $T_{i,in,hybrid}$, $T_{e,in,hybrid}$, and $V_{iL,X-line_drift}$ were calculated using formulas from Cassak and Shay (2007), Phan *et al.* (2014), and Doss *et al.* (2015).

and a factor of $\sim\!\!1.5$ and $\sim\!\!2$ difference in the electron and ion temperatures, respectively [Figs. 4(b)–4(j)]. The magnetic shear across the current sheet was $\sim\!\!62^\circ$, i.e., the guide field was 1.9 times the reconnecting magnetic field. Calculated for each individual spacecraft, the hybrid inflow ion Alfvén speed (V $_{AL}$) (Cassak and Shay, 2007) based on the two inflow densities and reconnecting magnetic field B_L ranges from $\sim\!114$ to 118 km/s for the four spacecraft.

In the spacecraft frame, there were tangential ion and electron flows outside the current sheet, and a small shear across the current sheet [Figs. 3(b)-3(e), 3(g)-3(j); Table I]. Doss *et al.* (2015) predicted that the X-line would move along the L direction at a drift speed given by

$$V_{drift} = (N_1 B_2 V_{L,1} + N_2 B_1 V_{L,2}) / (N_1 B_2 + N_2 B_1),$$

where N, B, and V_L are the density, magnetic field, and tangential flow in the inflow regions, with 1 and 2 denoting the two inflow regions. The predicted X-line drift speed along L is similar at the four spacecraft, ranging from 83 to 88 km/s (Table I), with an average of \sim 86 km/s. As will be shown in Sec. VII D, the current sheet normal speed in the spacecraft frame was \sim 220 km/s. Thus, the spacecraft trajectories through the current sheet were likely slanted [Fig. 2(1)].

Because the X-line likely drifted along L while the spacecraft traversed the current sheet one after the other, the effective coverage of the current sheet by the four spacecraft along L would be longer than

implied by a static X-line. The time from the first (MMS 4) to the last (MMS 1) spacecraft crossed the current sheet midplane ($B_L=0$) was 1.4 s. During that time, the X-line moved $\sim\!121\,km$ in the positive L-direction. Because the L separation between MMS 1 and 4 was $\sim\!42\,km$, the effective current sheet coverage by the four spacecraft along L would be $42+121=163\,km$, corresponding to 1.7 d_i (based on average $d_i\sim94\,km$, Table I).

VII. EVOLUTION OF THE RECONNECTION LAYER STRUCTURE WITH DISTANCE FROM THE X-LINE

The fortuitous ion-scale spacecraft separation along the outflow direction for this event made it possible to study the spatial evolution of the reconnection layer profiles in the EDR–IDR transition region within the $\sim\!\!1.7~d_i$ (along the outflow direction) covered by the four spacecraft. Noticeable differences in magnetic field, plasma, and electric field profiles were observed at the four spacecraft as presented below. The event reveals how quickly the structures of the diffusion region plasma and electromagnetic field evolve with downstream distance.

A. Magnetic field profiles

All spacecraft observed a rotation in B_L from $\sim +12$ to ~ -13 nT [Fig. 2(a)]. However, the four spacecraft observed slightly different B_L

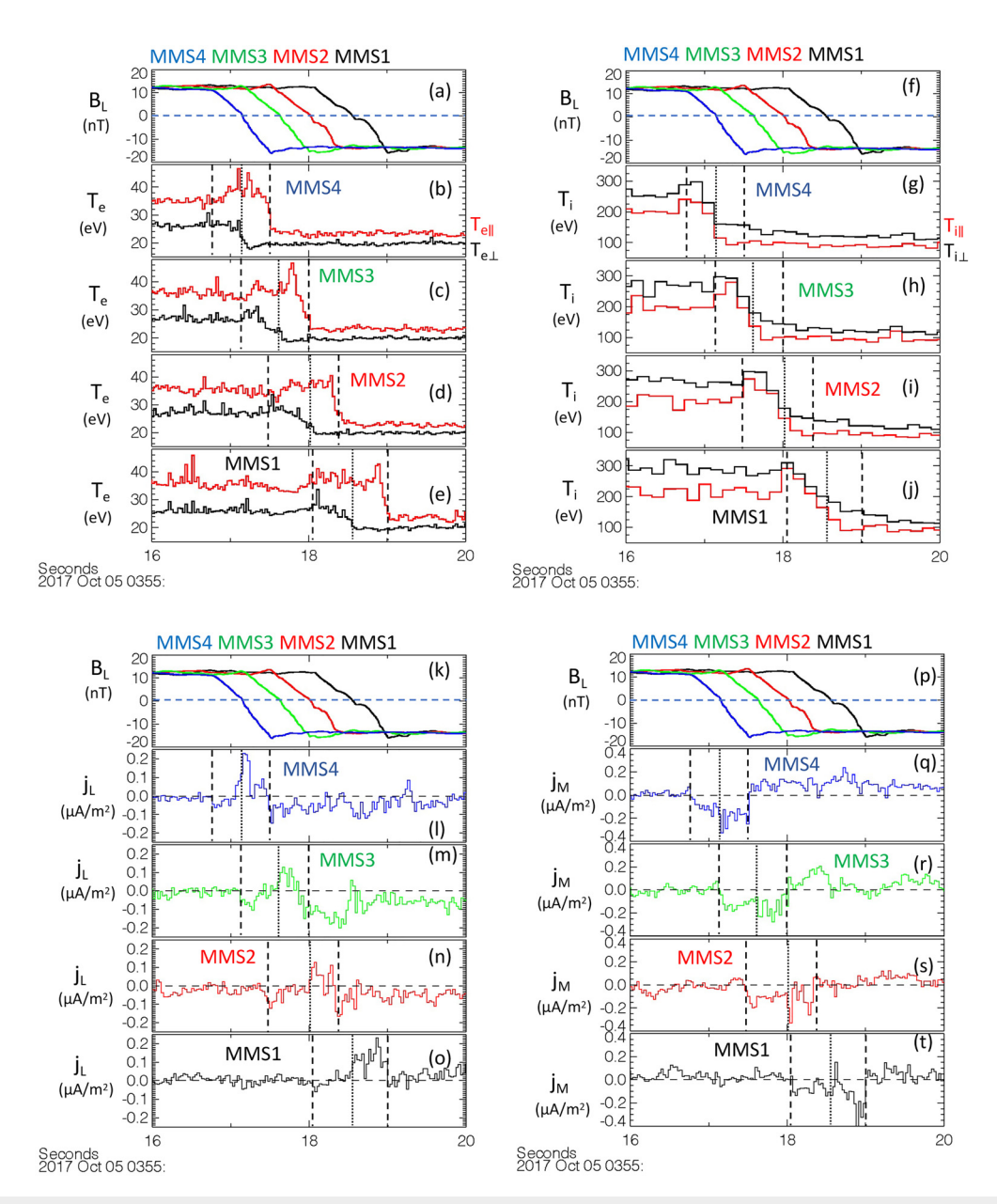


FIG. 4. Detailed multispacecraft observations of the thin current sheet in LMN coordinates. (a), (f), (k), and (p) Reconnecting magnetic field B_L for all four spacecraft, (b)–(e) and (g)–(j) electron and ion temperature for each spacecraft, (l)–(o), (q)–(t) current density along L and M. Vertical dashed lines in the time series mark the current sheet edges and the vertical dotted lines the current sheet midplane ($B_L = 0$).

profiles. The two spacecraft closer to the X-line, MMS4 (blue) and MMS3 (green), observed a B_L reversal that was nearly linear, while MMS2 (red) and MMS1 (black) observed a small plateau in the B_L reversal. Similar plateaus are predicted to occur in the exhaust downstream of the X-line where the current sheet is bifurcated (Petschek, 1964; Lin and Lee, 1994; Liu *et al.*, 2011) and are commonly observed in solar wind reconnection exhausts far downstream of the X-line (Phan *et al.*, 2006; 2020; Gosling and Szabo, 2008; Eriksson *et al.*, 2009; Mistry *et al.*, 2015). The present observations thus suggest that

the transition from a near-linear B_L profile to a more bifurcated current sheet can occur already within the IDR.

Some differences are also seen in the positive to negative bipolar (Hall) variation in B_M observed by all four spacecraft [Figs. 2(b)–2(e)]. While the amplitudes of the bipolar variation were similar, the width of the B_M perturbations (especially in the positive B_M variation) increased from MMS4 to MMS1, consistent with an increasing current sheet width with downstream distances. A dominant positive Hall B_M variation is expected for this event where the guide field is large and

positive (Pritchett, 2001; Eastwood et al., 2010b). Note that the positive B_M perturbation peaked inside the current sheet on the left side, whereas the negative B_M perturbation peaked right at the current sheet edge. This feature is likely a guide field effect and has been seen in simulations (e.g., Øieroset et al., 2016, Fig. 3l). All four spacecraft observed a brief break ("shoulder") during the B_M transition from positive to negative Hall magnetic field variation, indicating a small spatial separation between the bipolar Hall magnetic fields.

B_N was positive and oscillatory at all four spacecraft, and its average value did not appear to change with downstream distances [Figs. 2(g)-2(j)]. Interestingly, the B_N magnitude showed local maxima at the two edges of the current sheet, with a local minimum near the current sheet midplane ($B_L = 0$). Although there were other oscillations outside the current sheets, the fact that the local B_N maxima at the current sheet edges were seen by all four spacecraft suggests that they are a spatial feature of the reconnecting current sheet.

Similar B_N enhancements have been found in the electron separatrices of the EDR-IDR transition region, both in particle-in-cell simulations and in MMS data (Genestreti et al., 2020). Since ions are demagnetized in the IDR, electron convection carries magnetic flux from the inflow to outflow regions. The inflowing electrons are diverted along the magnetic separatrix toward the X-line and then cross the separatrix into the exhaust where they flow with super-Alfvenic velocity downstream. The flow toward the X-line and then down the exhaust is the Hall current loop. The electrons slow down as they cross the separatrix, and since the magnetic flux is frozen into the electrons in the ion diffusion region, there is a pileup of magnetic flux that leads to the enhanced B_N at the separatrices in Fig. 2. Similar peaks (overshoots) appear in B_L near the separatrices of some of the spacecraft data. While the Genestreti et al. (2020) case at the magnetopause had highly asymmetric returning Hall currents and B_N pileup occurred primarily on the magnetosheath (high density, weak magnetic field) separatrix of the current sheet, the B_N pileup of the present nearly symmetric event occurred on both sides of the reconnection exhaust.

The structure of B_N can also be understood in terms of the electron Hall current J_M that peaks at the separatrices, which for locations close to the X-line, are located slightly inward of the exhaust boundaries (e.g., Phan et al., 2016). The separatrix electron currents of the Hall current system are dominantly parallel to the local magnetic field, which has a large component B_M at the separatrices. As a consequence, there is a negative peak in J_M at the separatrices (slightly inward of the current sheet boundaries/dashed lines) that can be seen at some spacecraft, especially on the right side (Fig. 4). Because these electron-scale separatrix currents are tilted with respect to the axis of the outflow exhaust (L direction), the small jumps in the magnetic fields across the separatrix can be related using $\nabla \cdot B = 0$, which results in δB_N $\sim \tan(\theta) \delta B_L$ with θ being the angle between the separatrix and the L direction. The Hall currents $J_M < 0$ peak just inside the dashed lines marked in Fig. 4. They produce an increase in B_N and B_L just outside the entry separatrix and a drop inside. The phases of the two reverse on the exit separatrix. The resulting peak in B_N at the separatrix is seen by all spacecraft. The small increase (overshoot) in B_L just outside of the separatrices is only seen clearly on some of the separatrix crossings. As seen in Figs. 2(f)-2(j), B_L and B_N are correlated inside the current sheet adjacent to the current sheet edges, in agreement with the expected relation $\delta B_N \sim \tan(\theta) \delta B_L$. The estimated separatrix angle θ from this phase linkage between δB_L and δB_N ranges between 11° and 29° at the eight separatrix crossings, which corresponds to an aspect ratio $\delta B_I/\delta B_N$ between 0.2 and 0.55. We found no systematic variation of the separatrix angle with distance from the X-line.

B. Ion and electron outflows

There were distinct differences in the ion and electron outflows observed by the four spacecraft. The differences show a transition from electron-only outflow closer to the X-line to the emergence of ion outflow further downstream, as we now explain.

MMS1, located furthest downstream from the X-line, observed a negative enhancement in V_{iL} of ~ 30 km/s relative to an average V_L of 81 km/s outside the current sheet [Fig. 3(e)]. The ion outflow speed of ~30 km/s is substantially lower than the hybrid Alfvén speed of 116 km/s. MMS2, located second-furthest from the X-line, also observed an ion jet, reaching a magnitude of ~25 km/s relative to the average V_{iL} outside the current sheet [Fig. 3(d)]. On the other hand, MMS3 observed an even weaker jet, while MMS4, located closest to the X-line, did not observe a clear ion jet [Figs. 3(b) and 3(c)]. Thus, the observations indicate that the four MMS spacecraft captured the transition from no (or weak) ion jet closer to the X-line to the emergence of a sub-Alfvénic ion jet further downstream.

While the ion outflow was weak or non-existent at MMS4, the spacecraft closest to the X-line, a clear electron jet was observed at the current sheet midplane (B_L = 0) with an outflow speed reaching \sim 210 km/s relative to the external flow [Fig. 3(g)], indicating that MMS4 traversed a region where the electron reconnection jet was super ion Alfvénic (MMS4 hybrid V_{AL} = 118 km/s—see Table I). At MMS3, MMS2, and MMS1, the electron jet was less defined and the maximum outflow speed significantly lower than at MMS4 near midplane (~115–140 km/s, close to the ion Alfvén speed) [Figs. 3(h)–3(j)], suggesting a deceleration of V_{eL} with increasing distance from the X-line.

To examine the frozen-in conditions for ions and electrons, Figs. 3(q)-3(t) show that the perpendicular ion velocity and the $E \times B/B^2$ velocity along L did not agree inside the current sheet, indicating that the ions were not frozen-in at any of the four spacecraft. For electrons, except for some short time scale differences, the perpendicular electron velocity agreed reasonably well with $\mathbf{E} \times \mathbf{B}/\mathrm{B}^2$ inside the current sheet at all four spacecraft, suggesting that the electrons were mostly frozenin. Thus, based on the ion and electron velocity data alone, the four spacecraft likely crossed the IDR (where the ions are not frozen-in), but there is no clear evidence for EDR proper encounter. We do note that it is rare to directly observe large violation of the electron frozenin condition ($E = -V_e \times B$) even in previously reported EDR events. Instead, the presence of finite E $_{||}$ and/or positive $j\cdot (E\,+\,V_{e}\,\times\,B)$, together with non-gyrotropic electron distributions, has often been used to make the case for EDR encounters (e.g., Burch et al., 2016a, 2016b; Chen et al., 2016; Eriksson et al., 2016; Webster et al., 2018; Phan et al., 2018; Torbert et al., 2018). We will come back to this point in Sec. VII F, where we examine $E_{||}$ and $j \cdot (E + V_e \times B)$.

All spacecraft observed enhanced electron flows toward the Xline near the left edge of the currents sheet [Figs. 3(g)-3(j)]. This is consistent with electron inflow toward the X-line along the low density separatrix for guide field reconnection (Pritchett and Coroniti, 2004). A distinct bipolar density perturbation across the exhaust was observed, with a depletion followed by an enhancement [Figs. 3(1)-3(0)], consistent with the density structure in guide field reconnection (Pritchett and Coroniti, 2004; Drake *et al.*, 2005; Øieroset *et al.*, 2016; 2017; Eastwood *et al.*, 2018; Fox *et al.*, 2017).

C. Current density derived from the electron and ion measurements

The observed current density derived from the electron and ion measurements across the current sheet also shows some evolution with downstream distance from the X-line, particularly for the out-ofplane (M) component.

The out-of-plane component of the current density [Figs. 4(q)-4(t)] reached maxima of 0.3–0.4 μ A m⁻² inside the current sheet for all spacecraft. MMS4 [Fig. 4(q)], closest to the X-line, observed a j_M that was relatively stable across the current sheet, except for an enhancement near midplane, where the B_L profile was sharpest [Fig. 4(p)]. At MMS1, located farthest away from the X-line, two to three peaks were discernable in the j_M profile, suggesting that the current sheet was more bifurcated. The j_M profiles observed by the other two spacecraft were less clear but also suggest some level of bifurcation. Thus, overall the level of current sheet bifurcation seemed to increase with downstream distance. It is noted that generally, current density shows more structures than the corresponding magnetic field profiles. This is also the case here, where the bifurcated nature of the current sheet is clearer in the B_L profiles, which show a plateau near midplane.

The j_L profiles, on the other hand, were qualitatively similar at the four spacecraft, with a positive double-peak j_L enhancement inside the reconnection layer and negative values near the edges [Figs. 4(l)-4(o)]. This pattern is consistent with the predicted Hall current system [Sonnerup, 1979, see also Fig. 2(k)]. The brief minimum j_L interval between the two positive j_L peaks coincided with the B_M shoulder [Sec. VII A and Figs. 2(b)–2(e)], i.e., both the j_L and B_M observations seem to indicate a small, spatial gap between the two Hall current loops. The positive j_L peaks were observed to the right of the midplane, implying a shift in the Hall current pattern toward the high-density part of the exhaust, which is expected for guide field reconnection (e.g., Eastwood *et al.*, 2010b; Øieroset *et al.*, 2016).

D. Reconnection rate deduced four different ways

In this section, we estimate the reconnection rate by measuring (1) the normal magnetic field, (2) the opening angle of the current sheet, (3) the reconnection electric field E_M , and (4) the inflow velocity. Our findings will illustrate the challenge of determining the reconnection rate accurately.

Table I shows that the average B_N [across the exhaust including the two inflow intervals, see also Figs. 2(g)–2(j)] was in the range of 2.7–3.6 nT at the four spacecraft, with standard deviation in the range of 0.8–0.9 nT. Normalized to the average B_L in the inflow, the dimensionless reconnection rate was 0.20–0.27.

Assuming that the variation in M-direction is ignorable, the differences in the current sheet thickness at the four spacecraft provide a unique opportunity to roughly estimate the opening angle of the exhaust, and the implied reconnection rate. As discussed above in Sec. V, the duration of the current sheet increased gradually from MMS4 to MMS1, consistent with a widening of the exhaust with distance from the X-line. As stated above, the current sheet convected at a normal velocity $V_{\rm iN}$ of \sim 220 km/s. The observed current sheet crossing duration at MMS1, MMS2, MMS3, and MMS4 was 1.01, 0.94, 0.905,

and 0.760 s, respectively. This translates to an exhaust width (i.e., along the N direction) of 222 km at MMS1, 207 km at MMS2, 199 km at MMS3, and 167 km at MMS4. Taking the two extreme widths (at MMS 4 and 1), and the fact that the effective MMS 1 and 4 separation along L, Δ L, was 163 km, the estimated dimensionless reconnection rate is the difference between the exhaust half-width at MMS 1 and MMS 4, divided by Δ L, yielding a reconnection rate of 0.17.

The direct measurement of the reconnection electric field is challenging for this event where E_M was highly variable [Figs. 5(g)–5(j), green curves, see also Table I]. The average E_M in the current sheet and inflow regions at the four spacecraft was between -0.07 and $-0.25\,\text{mV/m}$. Normalized to the inflow B_L and V_{AL} , this yields a normalized reconnection rate of 0.03–0.11. However, while the negative sign of E_M is consistent with the reconnection electric field, the standard deviations of the mean E_M are much larger than the mean E_M themselves (Table I). Thus, we do not consider the estimated reconnection rate based on E_M to be meaningful.

Finally, we estimate the reconnection rate based on the inflow speed observed in the frame of the current sheet (e.g., Phan et al., 2006; Davis et al., 2006). First, Figs. 5(b)–5(e) show that there was a negative change in V_{iN} , ΔV_{iN} , across the current sheet at all four spacecraft, with V_{iN} ranging from $\sim\!-205$ to -210 km/s to the left of the current sheet, and $\sim\!-225$ to -235 km/s to the right of the current sheet. A negative ΔV_{iN} would be consistent with an inflow of $\sim\!15$ to 30 km/s, superimposed on the current sheet convective velocity V_{iN} of $\sim\!-220$ km/s. The normalized reconnection rate $V_{in,rec}/V_{AL}$ would be 0.13–0.26.

The reconnection rates of 0.13–0.27 from the different methods are within the range of previously reported values (e.g., Birn *et al.*, 2001; Phan *et al.*, 2001; Vaivads *et al.*, 2004; Fuselier *et al.*, 2010; Liu *et al.* 2017; 2018; Nakamura *et al.*, 2018; Genestreti *et al.*, 2018). However, the large uncertainties in the estimated reconnection rate show that even for this relatively clean event, the uncertainty in the estimated rate is more than a factor of 2.

E. Electric field E_N and E_L

All four spacecraft observed enhanced electric fields inside the current sheet, with the main enhancement seen in the normal component whose magnitude reached 3–5 mV/m [Figs. 5(g)–5(j), red curves]. While the polarity was variable, E_N was generally large and positive at the current sheet midplane where the electron outflow was observed, as expected for this large guide field event where $E_N \sim -V_{eL} \times B_M$ (Drake et al., 2009; Liu et al., 2014; Drake and Swisdak, 2014; Phan et al., 2018).

In terms of E_L [Figs. 5(g)–5(j), blue curves], one noticeable feature is the presence of a \sim 2 mV/m local enhancement around the left edge of the current sheet, and a negative \sim 1 mV/m field on the right edge. The amplitudes of the E_L fields are similar at the four spacecraft. The $|E_L|$ enhancements are likely associated with the electron inflows in the presence of a strong guide field: $E_L \sim V_{eN} \times B_M$. The electron inflow $|V_{eN}|$ (not shown) has local maxima near the separatrices (Burch et al., 2020), resulting in the $|E_L|$ enhancements.

F. Parallel electric field and J-E'

All spacecraft observed enhanced parallel electric fields inside the current sheet, with notably different cross-current sheet profiles [Figs. 5(l)–5(o)]. The most striking differences were seen in the DC field, with a $\sim\!\!250\,\text{ms}$ duration and $\sim\!\!-1\,\text{mV/m}$ magnitude $E_{||}$

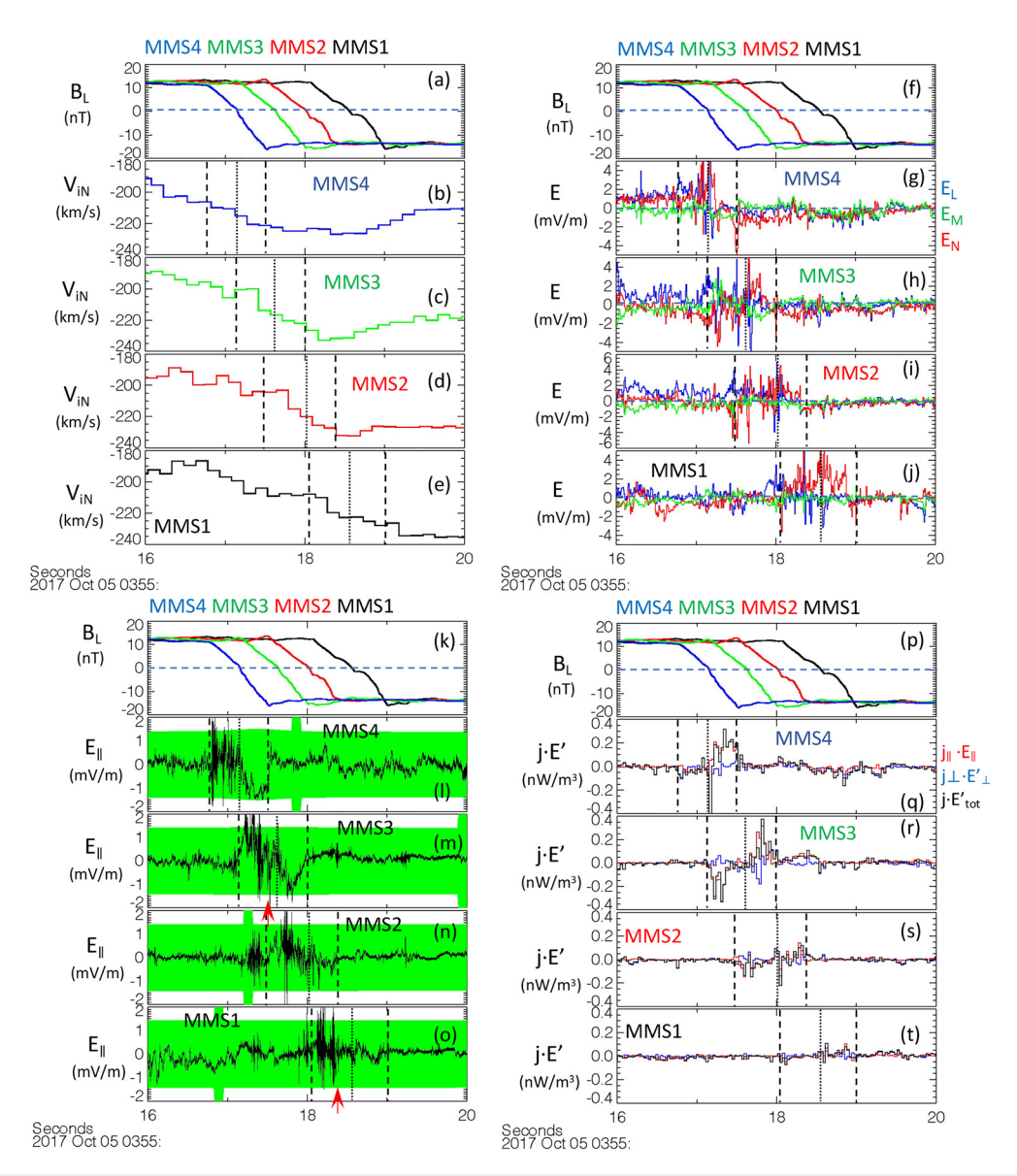


FIG. 5. Detailed multispacecraft observations of the thin current sheet in LMN coordinates. (a), (f), (k), and (p) Reconnecting magnetic field B_L , (b)–(e) V_{iN} for each spacecraft, (g)–(j) electric field, in the X-line frame, (l)–(o) $E_{||}$ for each spacecraft (black) with the uncertainty marked in green, (p)–(t) j-E'. Vertical dashed lines in the time series mark the current sheet edges and the vertical dotted lines the current sheet midplane ($B_L=0$). Red arrows in (m) and (o) mark the times when the double layers plotted in Fig. 6 were observed.

structure in the right half of the exhaust at MMS4 and MMS3, which was not present or significantly reduced at MMS2 and MMS1. The presence of finite $E_{||}$ implies that the "electron frozen-in condition" ($E' = E + V_e \times B = 0$) was violated. Similar DC $E_{||}$ structures have been reported in the EDR for large guide field events (Eriksson et al., 2016; Wilder et al., 2017; Phan et al., 2018). It is noted that DC $E_{||}$ variations with $\gtrsim 100$ ms time scales were associated with a $\pm \sim 1.5$ mV/m uncertainty for this event [green shaded area in Figs. 5(l)–5(o)]. Thus, one cannot rule out the possibility that the DC $E_{||}$ could be artificial.

Taking the measured $E_{||}$ at its face values, we examined $j \cdot E'$, the non-ideal magnetic to particle energy conversion parameter (Zenitani et al., 2011). Figures 5(q)-5(t) show that $j \cdot E'$ was larger at MMS 4 and 3, the spacecraft closer to the X-line, with positive enhancements up to 0.4 nW/m^3 , while $j \cdot E'$ observed by MMS1 and MMS2 was $<0.2 \text{ nW/m}^3$. The positive $j \cdot E'$ occurred in the right half of the current sheet. The dissipation was dominated by $j_{||} \cdot E_{||}$ (red curve), similar to what was found in previous studies of guide field reconnection (Wilder et al. 2018; Phan et al. 2018; Fox et al., 2018). Thus, if the \sim 250 ms $E_{||}$ structure is real, the observations imply that MMS 4 and 3 detected

significant dissipation, but it was much reduced less than 2 d_i downstream. The observed dissipation is a factor of 10–20 lower than dissipation observed in the EDR at the dayside magnetopause and magnetosheath (Burch *et al.*, 2016b; Eriksson *et al.*, 2016; Wilder *et al.*, 2017; Phan 2018), but similar to dissipation reported in the EDR in the magnetotail (Torbert *et al.*, 2018). Intervals of negative $\mathbf{j} \cdot \mathbf{E}'$ were also observed. The negative $\mathbf{j} \cdot \mathbf{E}'$ was confined to the left edge of the current sheet and was most prominent at MMS3.

High-frequency fluctuations with time scales ≤100 ms were not affected by the above-mentioned measurement uncertainty. All spacecraft observed high-frequency E|| fluctuations with amplitudes up to 2 mV/m [Figs. 5(l)-5(o)]. A large portion of the high-frequency variations were bipolar ∼1 ms period structures typical of electron phasespace holes, but unipolar E|| structures indicative of double layers (e.g., Ergun et al., 2009) were also observed. Two examples are shown in Fig. 6. A \sim 10 ms duration unipolar $E_{||}$ structure was observed by MMS1 at \sim 03:55:18.350 UT, adjacent to a series of \sim 1 ms electron phase-space holes [Fig. 6(a)]. Three similar double layers were seen on MMS3 near 03:55:17.520 UT, also with electron phase space holes nearby [Fig. 6(b)]. The abundant presence of electron holes at all four spacecraft [Figs. 5(1)-5(o)] suggests that their occurrence does not depend on the distance to the X-line, at least within the IDR. It remains to be seen whether the presence or absence of double layers are dependent on the distance to the X-line or not. Double layers are known to occur naturally in regions dominated by kinetic processes (Ergun et al., 2009) and have been observed in the auroral ionosphere (Ergun et al., 2001) and in the magnetotail plasma sheet (Ergun et al., 2009).

G. Electron and ion heating

In this section, we determine the ion and electron heating seen at the four spacecraft [Figs. 4(b)-4(j)] to see (1) if the degree of heating varies with distance from the X-line and (2) how the heating compares with previous findings of heating in magnetopause reconnection exhausts far downstream of the X-line.

Because the ion and electron temperatures had substantial asymmetries on the two sides of the current sheet, being twice as high on the left side, the determination of the temperature increase in the current sheet associated with heating has to be done with care.

Qualitatively, one can see that both parallel and perpendicular ion temperatures were higher in the current sheet compared to the inflow regions at all four spacecraft. For electrons, the main increase was in the parallel temperature. There was also a left-right asymmetry inside the current sheet: For the ions, both $T_{i\perp}$ and $T_{i\parallel}$ were enhanced primarily left of the midplane, whereas for the electrons, it appears that $T_{e\parallel}$ was more enhanced right of midplane, while $T_{e\perp}$ was slightly enhanced left of midplane. Such asymmetries could be due to the presence of a strong guide field (Drake *et al.*, 2005, 2009; Drake and Swisdak, 2014, Øieroset *et al.*, 2016).

To quantitatively assess the degree of heating, we determined the effective inflow temperature, as well as the average current sheet temperature. For asymmetric inflows, the effective inflow temperature is given by (Phan *et al.*, 2013, 2014)

$$T_{inflow} = [N_1 T_1/B_{L1} + \, N_2 T_2/B_{L2}]/[N_1/B_{L1} + \, N_2/BL_2], \label{eq:tinflow}$$

where N is the density, T is the total temperature $(2T_{\perp} + T_{||})/3$, B_{L} is the reconnecting component of the magnetic field, and the subscript "1" and "2" denote the two inflow regions. The effective inflow temperature at the four spacecraft is 24 eV for electrons and 151–158 eV for the ions (Table I).

The average temperature inside the current sheet was calculated using $\langle T_{exhaust} \rangle = \langle NT \rangle / \langle N \rangle$, where $\langle \ \rangle$ denotes averages over the entire current sheet, which takes into account the density variations across the layer (Phan et al., 2014). Table I shows that the average temperature in the current sheet was 26–27 eV for electrons, and 170–172 eV for the ions. Thus, the amount of electron and ion heating was 2–3 and 12–20 eV, respectively. The ratio of ion to electron heating was between 4 and 7. There does not seem to be a systematic change in heating with distance from the X-line, as the four spacecraft observed similar degree of heating.

Next, we compared the observed heating with predicted electron and ion heating from the empirical formula for magnetopause reconnection exhausts (far from the X-line): $\Delta T_e=0.017~m_iV_A^2$ (Phan et al., 2013), and $\Delta T_i=0.13~m_iV_A^2$ (Phan et al., 2014). The predicted heating, using the observed inflow parameters in Table I, is 2 eV for electrons and 17–19 eV for ions.

Thus, the heating seen in the IDR (and possibly EDR) in this event is similar to exhaust heating previously reported. This suggests that both ion and electron heating have reached the levels for the exhaust already in the IDR. This finding is somewhat surprising, especially for the ions, since the ions were not frozen-in in the IDR, and the ion jetting was substantially sub-Alfvénic. One would have expected little ion heating in the IDR.

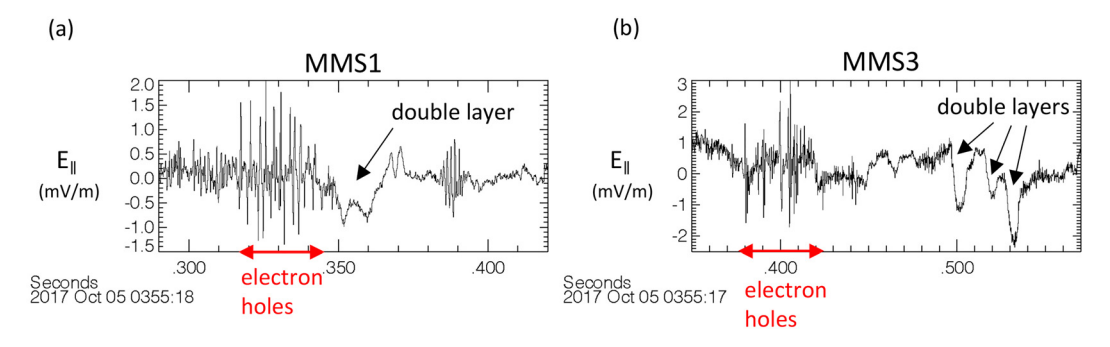


FIG. 6. Examples of electron phase space holes and double layers observed by MMS1 and MMS3 inside the reconnecting current sheet. (a) E_{\parallel} observed by MMS1, (b) E_{\parallel} observed by MMS3. Red arrows in Figs. 5(m) and 5(o) mark the observation times of the double layers.

VIII. SUMMARY AND DISCUSSION

We have presented an event where the four MMS spacecraft observed the spatial evolution of the reconnection layer profiles through the EDR–IDR transition region. The effective spacecraft separation in the outflow direction was about 1.7 d_i . We summarize the main findings here.

- MMS observed the transition from electron-only super ion-Alfvénic outflow closer to the X-line to the emergence of sub-Alfvénic ion outflow in the IDR. The emergence of sub-Alfvénic ion outflow coincided with a transition from a near-linear reconnecting magnetic field reversal to a more bifurcated current sheet (Petschek, 1964), suggesting that a B_L plateau starts to form already inside the IDR, i.e., before the exhaust is fully developed.
- 2. Enhancements of B_N were observed at the electron separatrices near the inflow portion of the Hall current loop, where the exhaust opens at a wide angle. The strong B_N regions were localized (<1 di) in N but extended at least 2 d_i downstream. Since this event was only weakly asymmetric in terms of the upstream density and B_L , it is therefore demonstrated that they are not unique to asymmetric geometries, as was previously reported (Genestreti *et al.*, 2020).
- 3. The two spacecraft closest to the X-line (MMS 4 and 3) detected enhanced DC $E_{||}$ and $\mathbf{j} \cdot \mathbf{E}'$, suggesting that they may have encountered the EDR. The electron distributions (not shown) did not show evidence for agyrotropy. This may not be unexpected for EDR in guide field reconnection (Genestreti *et al.*, 2017). DC parallel electric fields and associated enhanced dissipation became significantly weaker within less than 2 d_i downstream. It should be noted that the measured DC $E_{||}$ was associated with large measurement uncertainties; thus, there is a possibility that it is not real.
- 4. Ion and electron heating profiles were asymmetric (relative to midplane) within the current sheet. There were no noticeable differences in heating with distance from the X-line. Furthermore, the degree and ion and electron heating were similar to previously reported heating in magnetopause exhausts far downstream of the diffusion regions. These findings suggest that the ion and electron heating had reached exhaust-level values already inside the IDR, which is surprising especially for ions. This should be investigated in theoretical/simulation studies.
- 5. The dimensionless reconnection rate, estimated four different ways, was in the range 0.13–0.27, emphasizing an uncertainty of a factor of 2 or larger. These values are within the range of previous estimates from theory and observations (e.g., Birn *et al.*, 2001; Phan *et al.*, 2001; Vaivads *et al.*, 2004; Fuselier *et al.*, 2010; Liu *et al.*, 2017, 2018; Nakamura *et al.*, 2018; Genestreti *et al.*, 2018), but the spread in the estimated reconnection rate even for this relatively clean event illustrates the challenges of determining this parameter accurately. One challenge for future work will be to understand the connection between local features of the ion and electron diffusion regions (e.g., B_N at the separatrices/ current sheet edges) and the reconnection rate.

These unique observations of the spatial evolution of the crosscurrent-sheet profiles of the reconnection layer in the diffusion region were facilitated by the fortuitous ion-scale spacecraft separations in October 2017 and show that significant evolution of the magnetic reconnection diffusion region structures occurs over spatial scales of less than 2 d_i. The important, yet under-explored EDR-IDR transition region should be a target of future MMS investigations as the mission explores new orbit and spacecraft separation strategies.

ACKNOWLEDGMENTS

The reconnection event presented here was discovered in a database originally created by Goetz Paschmann and Stein Haaland, subsequently expanded in the framework of the International Space Science Institute (ISSI) Team 442. This research was supported by NASA Grant Nos. NNX16AG76G, NNX17AE12G, and 80NSSC18K1380 at UC Berkeley, and UKRI/STFC Grant No. ST/S000364/1 at Imperial College London.

AUTHOR DECLARATIONS

Conflict of Interest

The authors have no conflicts to disclose.

DATA AVAILABILITY

The data that support the findings of this study are openly available in MMS Science Data Center at lasp.colorado.edu/mms/sdc/public/ (Baker *et al.*, 2015).

REFERENCES

- Baker, D. N., Riesberg, L., Pankratz, C. K., Panneton, R. S., Giles, B. L., Wilder, F. D., and Ergun, R. E., "Magnetospheric multiscale instrument suite operations and data system," Space Sci. Rev. 199, 545 (2015).
- Birn, J., Drake, J. F., Shay, M. A., Rogers, B. N., Denton, R. E., Hesse, M., Kuznetsova, M., Ma, Z. W., Bhattacharjee, A., Otto, A., and Pritchett, P. L., "Geospace environmental modeling (GEM) magnetic reconnection challenge," J. Geophys. Res. 106(A3), 3715–3719, https://doi.org/10.1029/1999JA900449 (2001).
- Borg, A. L., Øieroset, M., Phan, T. D., Mozer, F. S., Pedersen, A., Mouikis, C., McFadden, J. P., Twitty, C., Balogh, A., and Rème, H., "Cluster encounter of a magnetic reconnection diffusion region in the near-Earth magnetotail on September 19, 2003," Geophys. Res. Lett. 32, L19105, https://doi.org/10.1029/2005GL023794 (2005).
- Burch, J. L. and Phan, T. D., "Magnetic reconnection at the dayside magnetopause: Advances with MMS," Geophys. Res. Lett. 43, 8327–8338, https:// doi.org/10.1002/2016GL069787 (2016).
- Burch, J. L., Moore, T. E., Torbert, R. B., and Giles, B. L., "Magnetospheric multi-scale overview and science objectives," Space Sci. Rev. 199, 5–21 (2016a).
- Burch, J. L., Torbert, R. B., Phan, T. D., Chen, L. J., Moore, T. E., Ergun, R. E., Eastwood, J. P., Gershman, D. J., Cassak, P. A., Argall, M. R. *et al.*, "Electronscale measurements of magnetic reconnection in space," Science 352(6290), aaf2939 (2016b).
- Burch, J. L., Webster, J. M., Hesse, M., Genestreti, K. J., Denton, R. E., Phan, T. D., Hasegawa, H., Cassak, P. A., Torbert, R. B., Giles, B. L. et al., "Electron inflow velocities and reconnection rates at Earth's magnetopause and magnetosheath," Geophys. Res. Lett. 47, e2020GL089082, https://doi.org/10.1029/2020GL089082 (2020).
- Cassak, P. A. and Shay, M. A., "Scaling of asymmetric magnetic reconnection: General theory and collisional simulations," Phys. Plasmas 14, 102114 (2007).
- Chen, L.-J., Hesse, M., Wang, S., Gershman, D., Ergun, R., Pollock, C., Torbert, R., Bessho, N., Daughton, W., Dorelli, J. et al., "Electron energization and mixing observed by MMS in the vicinity of an electron diffusion region during magnetopause reconnection," Geophys. Res. Lett. 43, 6036–6043, https://doi.org/10.1002/2016GL069215 (2016).
- Davis, M. S., Phan, T. D., Gosling, J. T., and Skoug, R. M., "Detection of oppositely directed reconnection jets in a solar wind current sheet," Geophys. Res. Lett. 33, L19102, https://doi.org/10.1029/2006GL026735 (2006).

- Doss, C. E., Komar, C. M., Cassak, P. A., Wilder, F. D., Eriksson, S., and Drake, J. F., "Asymmetric magnetic reconnection with a flow shear and applications to the magnetopause," J. Geophys. Res. 120, 7748–7763, https://doi.org/10.1002/2015JA021489 (2015).
- Drake, J. F. and Swisdak, M., "The onset of ion heating during magnetic reconnection with a strong guide field," Phys. Plasmas 21, 072903 (2014).
- Drake, J. F., Shay, M. A., Thongthai, W., and Swisdak, M., "Production of energetic electrons during magnetic reconnection," Phys. Rev. Lett. 94, 095001 (2005).
- Drake, J. F., Cassak, P. A., Shay, M. A., Swisdak, M., and Quataert, E., "A magnetic reconnection mechanism for ion acceleration and abundance enhancements in impulsive flares," Astrophys. J. 700, L16–L20 (2009).
- Eastwood, J. P., Phan, T. D., Øieroset, M., and Shay, M. A., "Average properties of the magnetic reconnection ion diffusion region in the Earth's magnetotail: The 2001–2005 cluster observations and comparison with simulations," J. Geophys. Res. 115, A08215, https://doi.org/10.1029/2009JA014962 (2010a).
- Eastwood, J. P., Shay, M. A., Phan, T. D., and Øieroset, M., "Asymmetry of the ion diffusion region Hall electric and magnetic fields during guide field reconnection: Observations and comparison with simulations," Phys. Rev. Lett. 104, 205001 (2010b).
- Eastwood, J. P., Mistry, R., Phan, T. D., Schwartz, S. J., Ergun, R. E., Drake, J. F., Øieroset, M., Stawarz, J. E., Goldman, M. V., Haggerty, C. et al., "Guide field reconnection: Exhaust structure and heating," Geophys. Res. Lett. 45, 4569–4577, https://doi.org/10.1029/2018GL077670 (2018).
- Ergun, R. E., Su, Y.-J., Andersson, L., Carlson, C. W., McFadden, J. P., Mozer, F. S., Newman, D. L., Goldman, M. V., and Strangeway, R. J., "Direct observation of localized parallel electric fields in a space plasma," Phys. Rev. Lett. 87, 045003 (2001).
- Ergun, R. E., Andersson, L., Tao, J., Angelopoulos, V., Bonnell, J., McFadden, J. P., Larson, D. E., Eriksson, S., Johansson, T., Cully, C. M. et al., "Observations of double layers in Earth's plasma sheet," Phys. Rev. Lett. 102, 155002 (2009).
- Eriksson, S., Gosling, J. T., Phan, T. D., Blush, L. M., Simunac, K. D. C., Krauss-Varban, D., Szabo, A., Luhmann, J. G., Russell, C. T., Galvin, A. B., and Acuña, M. H., "Asymmetric shear flow effects on magnetic field configuration within oppositely directed solar wind reconnection exhausts," J. Geophys. Res. 114, A07103, https://doi.org/10.1029/2008JA013990 (2009).
- Eriksson, S., Wilder, F. D., Ergun, R. E., Schwartz, S. J., Cassak, P. A., Burch, J. L., Chen, L.-J., Torbert, R. B., Phan, T. D., Lavraud, B. et al., "Magnetospheric multiscale observations of the electron diffusion region of large guide field magnetic reconnection," Phys. Rev. Lett. 117, 015001 (2016).
- Fargette, N., Lavraud, B., Øieroset, M., Phan, T. D., Toledo-Redondo, S., Kieokaew, R., Jacquey, C., Fuselier, S. A., Trattner, K. J., Petrinec, S. *et al.*, "On the ubiquity of magnetic reconnection inside flux transfer event-like structures at the Earth's magnetopause," Geophys. Res. Lett. 47, e2019GL086726, https://doi.org/10.1029/2019GL086726 (2020a).
- Fargette, N., Lavraud, B., Rouillard, A., Eastwood, J. P., Bale, S. D., Phan, T., Øieroset, M., Halekas, J. S., Kasper, J., Berthomier, M. et al., "Magnetic increases with central current sheets: Observations with Parker Solar Probe," Astron. Astrophys. 650, A11 (2020b).
- Fox, W., Sciortino, F., Stechow, A. v., Jara-Almonte, J., Yoo, J., Ji, H., and Yamada, M., "Experimental verification of the role of electron pressure in fast magnetic reconnection with a guide field," Phys. Rev. Lett. 118(12), 125002 (2017).
- Fox, W., Wilder, F. D., Eriksson, S., Jara-Almonte, J., Pucci, F., Yoo, J., Ji, H., Yamada, M., Ergun, R. E., Oieroset, M., and Phan, T. D., "Energy conversion by parallel electric fields during guide field reconnection in scaled laboratory and space experiments," Geophys. Res. Lett. 45, 12677–12684, https://doi.org/10.1029/2018GL079883 (2018).
- Fuselier, S. A., Petrinec, S. M., and Trattner, K. J., "Antiparallel magnetic reconnection rates at the Earth's magnetopause," J. Geophys. Res. 115, A10207, https://doi.org/10.1029/2010JA015302 (2010).
- Genestreti, K. J., Burch, J. L., Cassak, P. A., Torbert, R. B., Ergun, R. E., Varsani, A., Phan, T. D., Giles, B. L., Russell, C. T., Wang, S. *et al.*, "The effect of a guide field on local energy conversion during asymmetric magnetic reconnection: MMS observations," J. Geophys. Res. **122**, 11342–11353, https://doi.org/10.1002/2017JA024247 (2017).

- Genestreti, K. J., Nakamura, T. K. M., Nakamura, R., Denton, R. E., Torbert, R. B., Burch, J. L., Plaschke, F., Fuselier, S. A., Ergun, R. E., Giles, B. L., Russell, C. T. *et al.*, "How accurately can we measure the reconnection rate E_M for the MMS diffusion region event of 11 July 2017?," J. Geophys. Res. 123, 9130–9149, https://doi.org/10.1029/2018JA025711 (2018).
- Genestreti, K. J., Liu, Y.-H., Phan, T.-D., Denton, R. E., Torbert, R. B., Burch, J. L., Webster, J. M., Wang, S., Trattner, K. J., Argall, M. R. *et al.*, "Multiscale coupling during magnetopause reconnection: Interface between the electron and ion diffusion regions," J. Geogr. Res. 125, e2020JA027985 (2020).
- Gosling, J. T. and Szabo, A., "Bifurcated current sheets produced by magnetic reconnection in the solar wind," J. Geophys. Res. 113, A10103, https://doi.org/10.1029/2008JA013473 (2008).
- Hesse, M., Schindler, K., Birn, J., and Kuznetsova, M., "The diffusion region in collisionless magnetic reconnection," Phys. Plasmas 6, 1781 (1999).
- Kacem, I., Jacquey, C., Génot, V., Lavraud, B., Vernisse, Y., Marchaudon, A., Le Contel, O., Breuillard, H., Phan, T. D., Hasegawa, H. et al., "Magnetic reconnection at a thin current sheet separating two interlaced flux tubes at the Earth's magnetopause," J. Geophys. Res. 123, 1779–1793, https://doi.org/10.1002/2017JA024537 (2018).
- Lin, Y. and Lee, L. C., "Structure of reconnection layers in the magnetosphere," Space Sci. Rev. 65, 59–179 (1994).
- Liu, Y.-H., Drake, J. F., and Swisdak, M., "The effects of strong temperature anisotropy on the kinetic structure of collisionless slow shocks and reconnection exhausts. II. Theory," Phys. Plasmas 18, 092102 (2011).
- Liu, Y.-H., Daughton, W., Karimabadi, H., Li, H., and Peter Gary, S., "Do dispersive waves play a role in collisionless magnetic reconnection?," Phys. Plasmas 21, 022113 (2014).
- Liu, Y.-H., Hesse, M., Guo, F., Daughton, W., Li, H., Cassak, P. A., and Shay, M. A., "Why does steady-state magnetic reconnection have a maximum local rate of order 0.1?," Phys. Rev. Lett. 118(8), 085101 (2017).
- Liu, Y.-H., Hesse, M., Cassak, P. A., Shay, M. A., Wang, S., and Chen, L.-J., "On the collisionless asymmetric magnetic reconnection rate," Geophys. Res. Lett. 45, 3311–3318, https://doi.org/10.1002/2017GL076460 (2018).
- Mistry, R., Eastwood, J. P., Phan, T. D., and Hietala, H., "Development of bifurcated current sheets in solar wind reconnection exhausts," Geophys. Res. Lett. 42, 10513–10520, https://doi.org/10.1002/2015GL066820 (2015).
- Mozer, F. S., Bale, S. D., and Phan, T. D., "Evidence of diffusion regions at a subsolar magnetopause crossing," Phys. Rev. Lett. 89, 015002 (2002).
- Nagai, T., Shinohara, I., Fujimoto, M., Hoshino, M., Saito, Y., Machida, S., and Mukai, T., "Geotail observations of the Hall current system: Evidence of magnetic reconnection in the magnetotail," J. Geophys. Res. 106(A11), 25929–25949, https://doi.org/10.1029/2001JA900038 (2001).
- Nagai, T., Shinohara, I., Fujimoto, M., Matsuoka, A., Saito, Y., and Mukai, T., "Construction of magnetic reconnection in the near-Earth magnetotail with Geotail," J. Geophys. Res. 116, A04222, https://doi.org/10.1029/2010JA016283 (2011).
- Nakamura, T. K. M., Genestreti, K. J., Liu, Y.-H., Nakamura, R., Teh, W.-L., Hasegawa, H., Daughton, W., Hesse, M., Torbert, R. B., Burch, J. L., and Giles, B. L., "Measurement of the magnetic reconnection rate in the Earth's magnetotail," J. Geophys. Res. 123, 9150–9168, https://doi.org/10.1029/2018JA025713 (2018)
- Øieroset, M., Phan, T. D., Fujimoto, M., Lin, R. P., and Lepping, R. P., "In situ detection of collisionless recon-nection in the Earth's magnetotail," Nature 412, 414–417 (2001).
- Øieroset, M., Phan, T. D., Haggerty, C., Shay, M. A., Eastwood, J. P., Gershman, D. J., Drake, J. F., Fujimoto, M., Ergun, R. E., Mozer, F. S. et al., "MMS observations of large guide field symmetric reconnection between colliding reconnection jets at the center of a magnetic flux rope at the magnetopause," Geophys. Res. Lett. 43, 5536–5544, https://doi.org/10.1002/2016GL069166 (2016).
- Øieroset, M., Phan, T. D., Shay, M. A., Haggerty, C. C., Fujimoto, M., Angelopoulos, V., Eastwood, J. P., and Mozer, F. S., "THEMIS multispacecraft observations of a reconnecting magnetosheath current sheet with symmetric boundary conditions and a large guide field," Geophys. Res. Lett. 44, 7598–7606, https://doi.org/10.1002/2017GL074196 (2017).
- Øieroset, M., Phan, T. D., Drake, J. F., Eastwood, J. P., Fuselier, S. A., Strangeway, R. J., Haggerty, C., Shay, M. A., Oka, M., Wang, S. et al., "Reconnection with magnetic flux pileup at the interface of converging jets at the magnetopause,"

- Geophys. Res. Lett. **46**, 1937–1946, https://doi.org/10.1029/2018GL080994 (2019).
- Petschek, H. E., "Magnetic annihilation," in AAS-NASA Symposium on the Physics of Solar Flares (NASA Spec. Publications, 1964), p. 425.
- Phan, T.-D., Sonnerup, B. U. Ö., and Lin, R. P., "Fluid and kinetics signatures of reconnection at the dawn tail magnetopause: Wind observations," J. Geophys. Res. 106(A11), 25489–25501, https://doi.org/10.1029/2001JA900054 (2001).
- Phan, T. D., Gosling, J. T., Davis, M. S., Skoug, R. M., Øieroset, M., Lin, R. P., Lepping, R. P., McComas, D. J., Smith, C. W., Reme, H., and Balogh, A., "A magnetic reconnection X-line extending more than 390 Earth radii in the solar wind," Nature 439(12), 04393 (2006).
- Phan, T. D., Shay, M. A., Gosling, J. T., Fujimoto, M., Drake, J. F., Paschmann, G., Oieroset, M., Eastwood, J. P., and Angelopoulos, V., "Electron bulk heating in magnetic reconnection at Earth's magnetopause: Dependence on the inflow Alfvén speed and magnetic shear," Geophys. Res. Lett. 40, 4475–4480, https://doi.org/10.1002/grl.50917 (2013).
- Phan, T. D., Drake, J. F., Shay, M. A., Gosling, J. T., Paschmann, G., Eastwood, J. P., Oieroset, M., Fujimoto, M., and Angelopoulos, V., "Ion bulk heating in magnetic reconnection exhausts at Earth's magnetopause: Dependence on the inflow Alfvén speed and magnetic shear angle," Geophys. Res. Lett. 41, 7002–7010, https://doi.org/10.1002/2014GL061547 (2014).
- Phan, T. D., Eastwood, J. P., Cassak, P. A., Øieroset, M., Gosling, J. T., Gershman, D. J., Mozer, F. S., Shay, M. A., Fujimoto, M., Daughton, W. et al., "MMS observations of electron-scale filamentary currents in the reconnection exhaust and near the X line," Geophys. Res. Lett. 43, 6060–6069, https://doi.org/10.1002/2016GL069212 (2016).
- Phan, T. D., Eastwood, J. P., Shay, M. A., Drake, J. F., Sonnerup, B. U. Ö., Fujimoto, M., Cassak, P. A., Øieroset, M., Burch, J. L., Torbert, R. B. et al., "Electron magnetic reconnection without ion coupling in Earth's turbulent magnetosheath," Nature 557, 202–206 (2018).
- Phan, T. D., Bale, S. D., Eastwood, J. P., Lavraud, B., Drake, J. F., Oieroset, M., Shay, M. A., Pulupa, M., Stevens, M., MacDowall, R. J. et al., "Parker Solar Probe in situ observations of magnetic reconnection exhausts during encounter 1," Astrophys. J. Suppl. Ser. 246(2), 34 (2020).
- Pollock, C., Moore, T., Jacques, A., Burch, J., Gliese, U., Saito, Y., Omoto, T., Avanov, L., Barrie, A., Coffey, V. et al., "Fast plasma investigation for magnetospheric multiscale," Space Sci. Rev. 199, 331 (2016).
- Pritchett, P. L., "Geospace environment modeling magnetic reconnection challenge: Simulations with a full particle electromagnetic code," J. Geophys. Res. 106(A3), 3783–3798, https://doi.org/10.1029/1999JA001006 (2001).
- Pritchett, P. L. and Coroniti, F. V., "Three-dimensional collisionless magnetic reconnection in the presence of a guide field," J. Geophys. Res. 109, A01220, https://doi.org/10.1029/2003JA009999 (2004).
- Runov, A., Nakamura, R., Baumjohann, W., Treumann, R. A., Zhang, T. L., Volwerk, M., Vörös, Z., Balogh, A., Glassmeier, K.-H., Klecker, B. *et al.*, "Current sheet structure near magnetic X-line observed by cluster," Geophys. Res. Lett. **30**, 1579, https://doi.org/10.1029/2002GL016730 (2003).
- Russell, C. T. and Qi, Y., "Flux ropes are born in pairs: An outcome of interlinked, reconnecting flux tubes," Geophys. Res. Lett. 47, e2020GL087620, https://doi.org/10.1029/2020GL087620 (2020).

- Russell, C. T., Anderson, B. J., Baumjohann, W., Bromund, K. R., Dearborn, D., Fischer, D., Le, G., Leinweber, H. K., Leneman, D., Magnes, W., and Means, J. D., "The magnetospheric multiscale magnetometers," Space Sci. Rev. 199, 189–256 (2014).
- Shay, M. A., Drake, J. F., Denton, R. E., and Biskamp, D., "Structure of the dissipation region during collisionless magnetic reconnection," J. Geophys. Res. 103(A5), 9165–9176, https://doi.org/10.1029/97JA03528 (1998).
- Shay, M. A., Drake, J. F., Rogers, B. N., and Denton, R. E., "The scaling of collisionless, magnetic reconnection for large systems," Geophys. Res. Lett. 26, 2163, https://doi.org/10.1029/1999GL900481 (1999).
- Sonnerup, B. U. Ö., "Magnetic field reconnection," in *Solar System Plasma Physics*, edited by Lanzerotti, L. T., Kennel, C. F., and Parker, E. N. (North-Holland, New York, 1979), Vol. III, pp. 45–108.
- Sonnerup, B. U. Ö. and Cahill, L. J., Jr., "Magnetopause structure and attitude from Explorer 12 observations," J. Geophys. Res. 72(1), 171–183, https:// doi.org/10.1029/JZ072i001p00171 (1967).
- Torbert, R. B., Russell, C. T., Magnes, W., Ergun, R. E., Lindqvist, P.-A., LeContel, O., Vaith, H., Macri, J., Myers, S., Rau, D. et al., "The FIELDS instrument suite on MMS: Scientific objectives, measurements, and data products," Space Sci. Rev. 199, 105–135 (2014).
- Torbert, R. B., Burch, J. L., Giles, B. L., Gershman, D., Pollock, C. J., Dorelli, J., Avanov, L., Argall, M. R., Shuster, J., Strangeway, R. J. *et al.*, "Estimates of terms in Ohm's law during an encounter with an electron diffusion region," Geophys. Res. Lett. **43**, 5918–5925, https://doi.org/10.1002/2016GL069553 (2016).
- Torbert, R. B., Burch, J. L., Giles, B. L., Gershman, D., Pollock, C. J., Dorelli, J., Avanov, L., Argall, M. R., Shuster, J., Strangeway, R. J. *et al.*, "Electron-scale dynamics of the diffusion region during symmetric magnetic reconnection in space," Science **362**, 1391–1395 (2018).
- Vaivads, A., Khotyaintsev, Y., André, M., Retinò, A., Buchert, S., Rogers, B., Décréau, P., Paschmann, G., and Phan, T., "Structure of the magnetic reconnection diffusion region from four-spacecraft observations," Phys. Rev. Lett. 93(10), 105001 (2004).
- Vasyliunas, V. M., "Theoretical models of magnetic field line merging," Rev. Geophys. 13(1), 303–336, https://doi.org/10.1029/RG013i001p00303 (1975).
- Webster, J. M., Burch, J. L., Reiff, P. H., Daou, A. G., Genestreti, K. J., Graham, D. B., Torbert, R. B., Ergun, R. E., Sazykin, S. Y., Marshall, A. *et al.*, "Magnetospheric multiscale dayside reconnection electron diffusion region events," J. Geophys. Res. 123, 4858–4878, https://doi.org/10.1029/2018JA025245 (2018).
- Wilder, F. D., Ergun, R. E., Eriksson, S., Phan, T. D., Burch, J. L., Ahmadi, N., Goodrich, K. A., Newman, D. L., Trattner, K. J., Torbert, R. B. *et al.*, "Multipoint measurements of the electron jet of symmetric magnetic reconnection with a moderate guide field," Phys. Rev. Lett. 118, 265101 (2017).
- Wilder, F. D., Ergun, R. E., Burch, J. L., Ahmadi, N., Eriksson, S., Phan, T. D., Goodrich, K., Shuster, J., Rager, A., Torbert, R. *et al.*, "The role of the parallel electric field in electron-scale dissipation at reconnecting currents in the magnetosheath," J. Geophys. Res. **123**, 6533–6547, https://doi.org/10.1029/2018JA025529 (2018).
- Zenitani, S., Hesse, M., Klimas, M., and Kuznetsova, M., "New measure of the dissipation region in collisionless magnetic reconnection," Phys. Rev. Lett. 106, 195003 (2011).